JOURNAL OF GEOPHYSICAL RESEARCH, VOL. 105, NO. B4, PAGES 8279–8296, APRIL 10, 2000

# The Bouvet triple junction, 20 to 10 Ma, and extensive transtensional deformation adjacent to the Bouvet and Conrad transforms

Neil C. Mitchell[1]

Department of Earth Sciences, Oxford University, Oxford, England

Roy A. Livermore

British Antarctic Survey, Cambridge, England

Paola Fabretti and Gabriela Carrara

Istituto di Geologia Marina, Consiglio Nazionale delle Ricerche, Bologna, Italy

**Abstract.** The Bouvet triple junction has been proposed to have evolved as a ridge-fault-fault (RFF) type between 20 and 10 Ma, connecting the southernmost Mid-Atlantic Ridge (SMAR) with the Bouvet and Conrad transforms, to the east and west, respectively. We surveyed immediately north of these two transforms with side-scan and multibeam sonars, on seafloor that would have originally been created at the SMAR close to its junction with the two transforms. The sonar data reveal that SMAR fabrics on the Bouvet and Conrad sides, when corrected for plate rotation, are parallel to each other, so they were most likely formed at the same spreading ridge and confirm that the triple junction was indeed RFF. Our second major result is that the SMAR fabrics are extensively crosscut by normal faults, over most of the 400 km surveyed along both transforms and most intensely north of the Bouvet transform. Growth faults and faults affecting the sediment surface in multichannel seismic images show that the deformation has been long-lived and is probably ongoing. Since the orientations of the crosscutting faults are similar to those of shear zone tension fractures, we interpret these areas to be transtensional zones. This extent of deformation adjacent to major oceanic transforms is rare, and we develop a number of ideas to explain its origin.

## 1. Introduction

The Bouvet triple junction (Figures 1, 2a, and 2b) has been a focus of interest and speculation since it was first appreciated that the velocity space diagram for relative motion between Africa (AFR), Antarctica (ANT), and South America (SAM) is almost isosceles and therefore the triple junction could have evolved as either ridge-ridge-ridge (RRR) or ridge-fault-fault (RFF) [*Forsyth*, 1975; *Johnson et al.*, 1973; *Sclater et al.*, 1976]. These two configurations are shown schematically in the top of Figure 2a. In RFF mode the southernmost Mid-Atlantic Ridge (SMAR) is connected to two transform faults which form the plate boundaries of ANT with SAM and AFR. The triple junction velocity J coincides with ANT in RFF mode so the SMAR and J are stationary in the reference frame of ANT. The Southwest Indian Ridge (SWIR) and South American-Antarctic Ridge (SAAR), drawn bisecting the AFR-ANT and SAM-ANT vectors, diverge at a little less than the sum of their half spreading rates. In RRR mode the SMAR is connected to the extreme spreading segments of the SAAR and SWIR, and the triple junction velocity J lies far outside the velocity triangle, predicting rapid northward motion if spreading on all three ridges is symmetric and normal [*Patriat and Courtillot*, 1984]. Detailed studies with sonars [e.g., *Mitchell*, 1991] have since shown that spreading adjacent to triple junctions commonly involves obliquely oriented ridges, so rapid northward motion of J is not necessarily expected. Mapping in the 1970s [*Sclater et al.*, 1976] with wide-beam echo sounders and magnetometers was unable to show whether the Bouvet triple junction is presently RRR or RFF due to insufficient data resolution. Indeed, recent sonar data show that it is a complex area of distributed deformation dominated by a large seamount, Spiess Ridge, and the present junction is not easily classified as RRR or RFF [*Ligi et al.*, 1997; *Mitchell and Livermore*, 1998a,b].

*Sclater et al.* [1976] suggested that if the triple junction were RFF between chrons C6 and C5, this could have permitted growth of the Conrad and Bouvet transforms and therefore may explain their current lengths, since the SAAR and SWIR would have diverged at a little less than the sum of their half spreading rates as the transforms grew. Plate reconstructions by *Lawver et al.* [1985] suggested that predominantly RFF modes over the past 60-65 Myr may have led to the present generally oblique orientations of the SAAR and SWIR, which both have short spreading segments offset by long transforms. *Apotria and Gray* [1985] proposed that alternation between RRR and RFF occurred because of distortion of the triple junction velocity triangle as the junction migrated with respect to the plate rotation poles, alternately favoring RRR and RFF modes. *Kleinrock and Phipps Morgan* [1988] proposed an alternative mechanical explanation in which stresses near the plate boundaries surrounding the triple

[1]Now at Department of Earth Sciences, Cardiff University, Cardiff, Wales.



Paper number 1999JB900399.
0148-0227/00/1999JB900399$09.00

junction encouraged mode changes between RRR and RFF. *Barker and Lawver* [1988], however, suggested that the present configuration of short spreading segments separated by long transform offsets along the SAAR may have replaced a system of shorter WNW-ESE trending offsets at around C6 (20 Ma), casting doubt on this simple mode switching mechanism, which is also not supported by spreading fabrics in the marine gravity field [*Sandwell and Smith*, 1997]. In this study we address the configuration of the triple junction between approximately 20 and 10 Ma and confirm that it was most likely RFF for this period.

Deformation near major oceanic transforms is relatively common due to changes in direction of relative plate motion. Where changes cause shortening across transforms, thrusting and uplift can occur, such as at the Romanche transform [*Bonatti et al.*, 1994]. Where plate motions cause extension, the deformation is commonly confined to the transform valley where the lithosphere is presumably weak, leading to normal faulting, volcanism ("leaky" transforms) and short en-echelon spreading segments [e.g., *Tucholke and Schouten*, 1989]. Broadly distributed transtensional deformation, such as found here, is more rare; *Taylor et al.*'s [1994] review of oceanic transtensional zones included only one comparably large zone adjacent to a transform, a 50 by 20 km zone adjacent to the Willaumez transform. In view of the unique nature of these deformation zones, we devote part of this paper to describing the observations, which are principally side-scan sonar images and bathymetry, collected with the Hawaii-MR1 sonar [*Rognstad*, 1992] during a cruise of RRS *James Clark Ross* in early 1995 (Figure 2b), multichannel seismic and multibeam sonar data from a 1994 cruise of the R/V *Strakhov* and Simrad EM12 multibeam bathymetry from a 1996 cruise of the R/V *Gelendzhik* [*Ligi et al.*, 1997].

## 2. Observations

### 2.1. Bouvet Transform

**2.1.1. Multibeam echo sounder bathymetry data.** A shaded relief view of bathymetry around the Bouvet transform is shown in Figure 3a, derived from Simrad EM12 multibeam sonar data [*Ligi et al.*, 1997]. Figure 3b is an interpretation. The transform is typical of slow-spreading ridges, with a ~2 km deep valley, steep walls gullied by mass wasting, and an almost flat sedimented valley floor. The principal transform displacement zone (PTDZ) runs along the valley floor with an orientation, 043°-044°, slightly north of the 047.6° orientation predicted by the NUVEL-1A plate model [*DeMets et al.*, 1994].

Beyond the transform valley, Figure 3a shows a broad zone of deformation. The zone is bounded along its northwest side, 60 km from the Bouvet PTDZ, by several overlapping southwest-northeast trending grabens, which form a general bathymetric depression subparallel to the Bouvet transform (e.g., at 54°05'S, 1°10'E). The northernmost graben is connected to the transform valley by a series of east-west trending, southdipping escarpments interpreted as normal faults which breach the northern transform valley wall near 54°00'S, 2°30'E, at a point 140 km from the summit of Spiess Ridge, thus defining the area of most intense deformation as 140 by 60 km. Internally, the zone has mostly southdipping, east-west trending normal faults, although some southwest-northeast trending faults also occur. At the transform valley walls, some of the faults curve abruptly to be perpendicular to the transform. An east-west elongated block at 54°20'S, 1°30'E has fabrics oriented 10° clockwise of those elsewhere along the deformation zone, which might represent an original orientation or block rotation. Some structures lying southeast of the transform valley have trends oblique to the expected ~135° SWIR abyssal hill direction and may have a similar origin to those to the northwest.

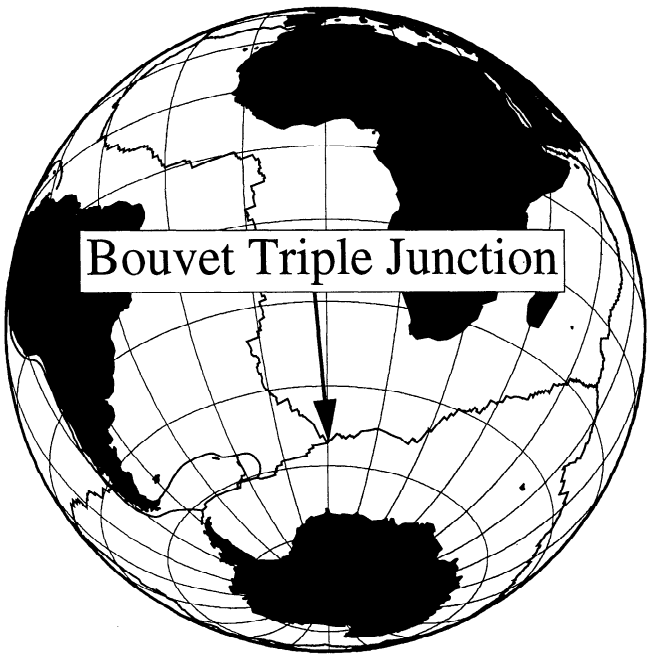


**Figure 1.** Location of the triple junction in the South Atlantic.

**2.1.2. Hawaii-MR1 side-scan sonar images and bathymetry.** An example of MR1 sidescan sonar images and bathymetry collected adjacent to the Bouvet transform is shown in Figure 4, and Figure 5b shows interpreted lineaments in an oblique Mercator projection. Figure 4 shows a typical north-south trending SMAR fabric, which is cut by a series of east-west trending, south facing normal fault scarps. The vertical relief on the scarps reaches more than 400 m and the continuity of acoustic shadows indicates that these faults crosscut, and therefore postdate, the SMAR fabric. Although less common northeast of Figure 4 due to sedimentation, some further crossing structures were also observed on older seafloor (Figure 5). One focal mechanism from the Harvard centroid moment tensor database (Figure 2b) is consistent with continued activity of these faults, while other transform valley earthquakes have transcurrent mechanisms.

**2.1.3. Multichannel seismic images.** A multichannel seismic line shot across the Bouvet transform (Figure 3b) gives some clues to the history of deformation. Within a small perched basin immediately southeast of the Bouvet transform valley (Figure 6a), the oceanic basement appears to be displaced by extensional faults bounding southward tilted blocks. Sediment in the basin contains two unconformities, A and B (Figure 6b), which correlate with the faults and suggest the following evolution. Sediment between basement and unconformity A was deposited while the two northernmost faults were active, sediment between unconformities A and B was deposited while activity migrated to the southern fault, and sediment above unconformity B is undeformed so the faults here are presently inactive.

The transform valley is filled by sediment to a thickness of ~1.5 km (Figure 7), assuming a $P$ wave velocity of 2 km/s, and possibly to 2 km if the reflectors at 9 s are not artifacts. We

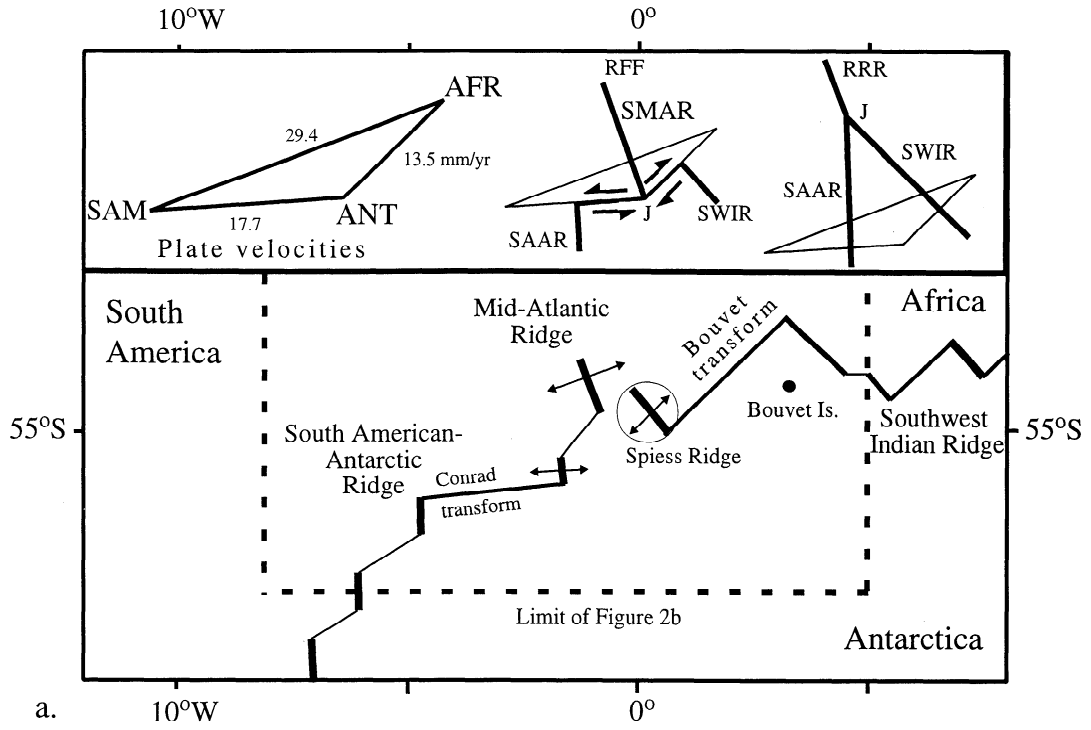


**Figure 2a.** Present geometry of the Bouvet triple junction and the Conrad and Bouvet transforms. The southernmost Mid-Atlantic Ridge is currently separated from the Conrad transform by a small spreading segment of the South American-Antarctic Ridge and an oblique transtensional rift basin (fine line) and from the Bouvet transform by Spiess Ridge, a large seamount [*Ligi et al.*, 1997; *Mitchell and Livermore*, 1998a, b]. The inset (top left) shows the triple junction velocity space diagram calculated from the NUVEL-1A plate model [*DeMets et al.*, 1994] and (top center and right) ridge-fault-fault (RFF) and ridge-ridge-ridge (RRR) configurations predicted from the velocity triangle [*Johnson et al.*, 1973; *Sclater et al.*, 1976]. The diagram represents South America (SAM), Africa (AFR), Antarctica (ANT), southernmost Mid-Atlantic Ridge (SMAR), South American-Antarctic Ridge (SAAR), Southwest Indian Ridge (SWIR), and triple junction (J).

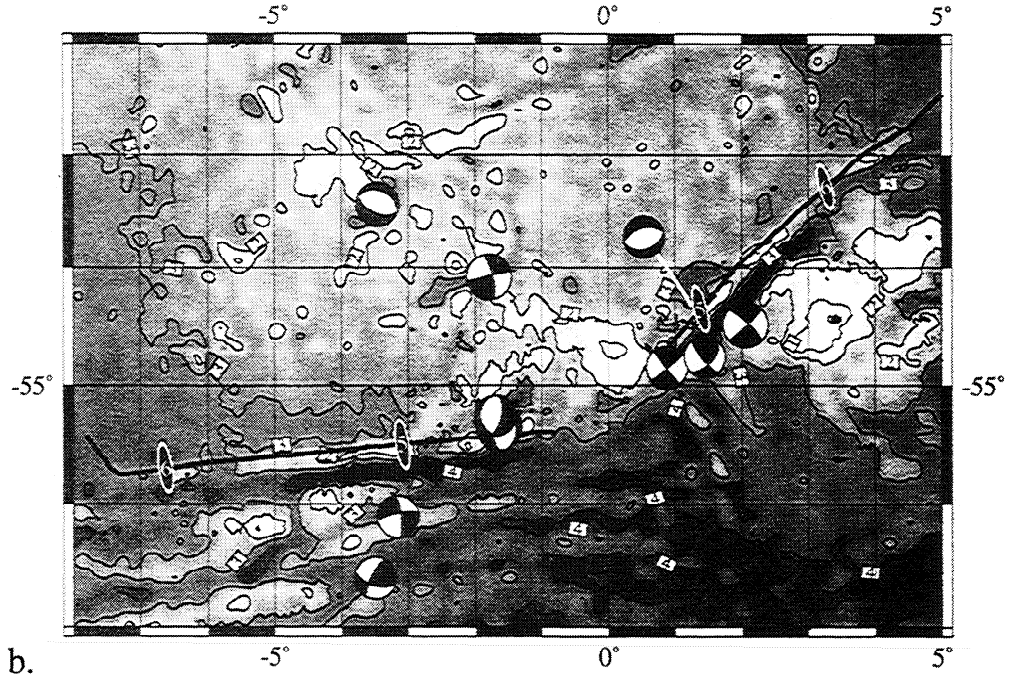


**Figure 2b.** Regional bathymetry derived from the marine gravity field [*Smith and Sandwell*, 1997] with depths in kilometers and contours every 1 km (see Figure 2a for plate geometry). The two bold lines show survey tracks of RRS *James Clark Ross* run adjacent to the Conrad and Bouvet transforms. The four highlighted black ellipses are identifications of chrons C5n.1n and C6n, oriented parallel to SMAR fabrics in MR1 data. Focal mechanisms are best fit double-couple mechanisms from the Harvard centroid moment tensor solution database [*Dziewonski et al.*, 1981; *Dziewonski and Woodhouse*, 1983] shown with compressional quadrants shaded. The normal first motion shown offset from its epicenter (white line) occurs in the transtensional zone discussed in the text.

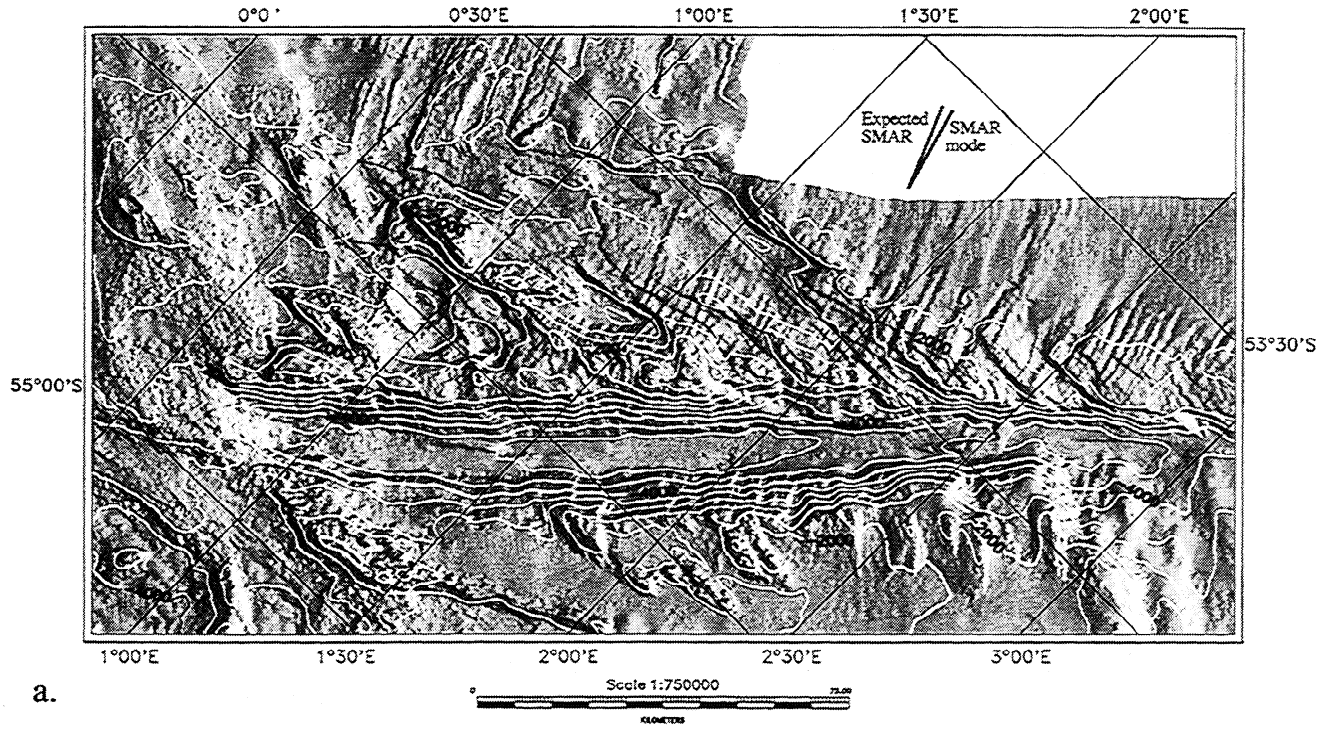


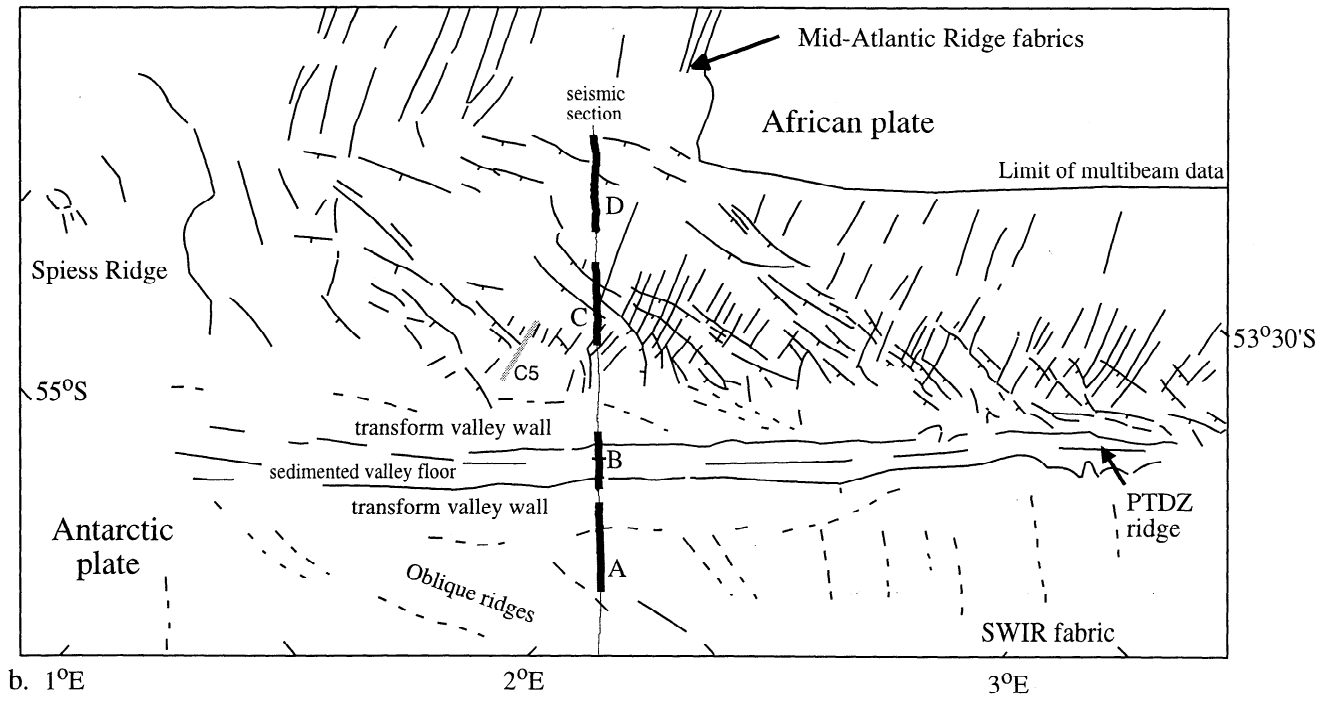


**Figure 3.** (a) A shaded relief image of the Bouvet transform derived from multibeam bathymetry collected on the R/V *Strakhov* in 1994 and R/V *Gelendzhik* in 1996 [*Ligi et al.*, 1997]. Contours are drawn every 500 m. The image is in an oblique Mercator projection with a projection equator parallel to AFR-ANT motion predicted by the NUVEL-1A plate model [*DeMets et al.*, 1994]. The two lines at the top right show (left line) the trend of the southernmost Mid-Atlantic Ridge (SMAR) predicted from AFR-SAM motion for C6-C5 [*Nankivell*, 1997] and (right line) the observed modal trend in MR1 sonar data adjacent to the transform valley. (b) Structural interpretation of the bathymetry. The annotated line locates the seismic profiles in Figures 6-9. The shaded bar immediately to the left of this line marks our interpreted young edge of chron C5n.1n.

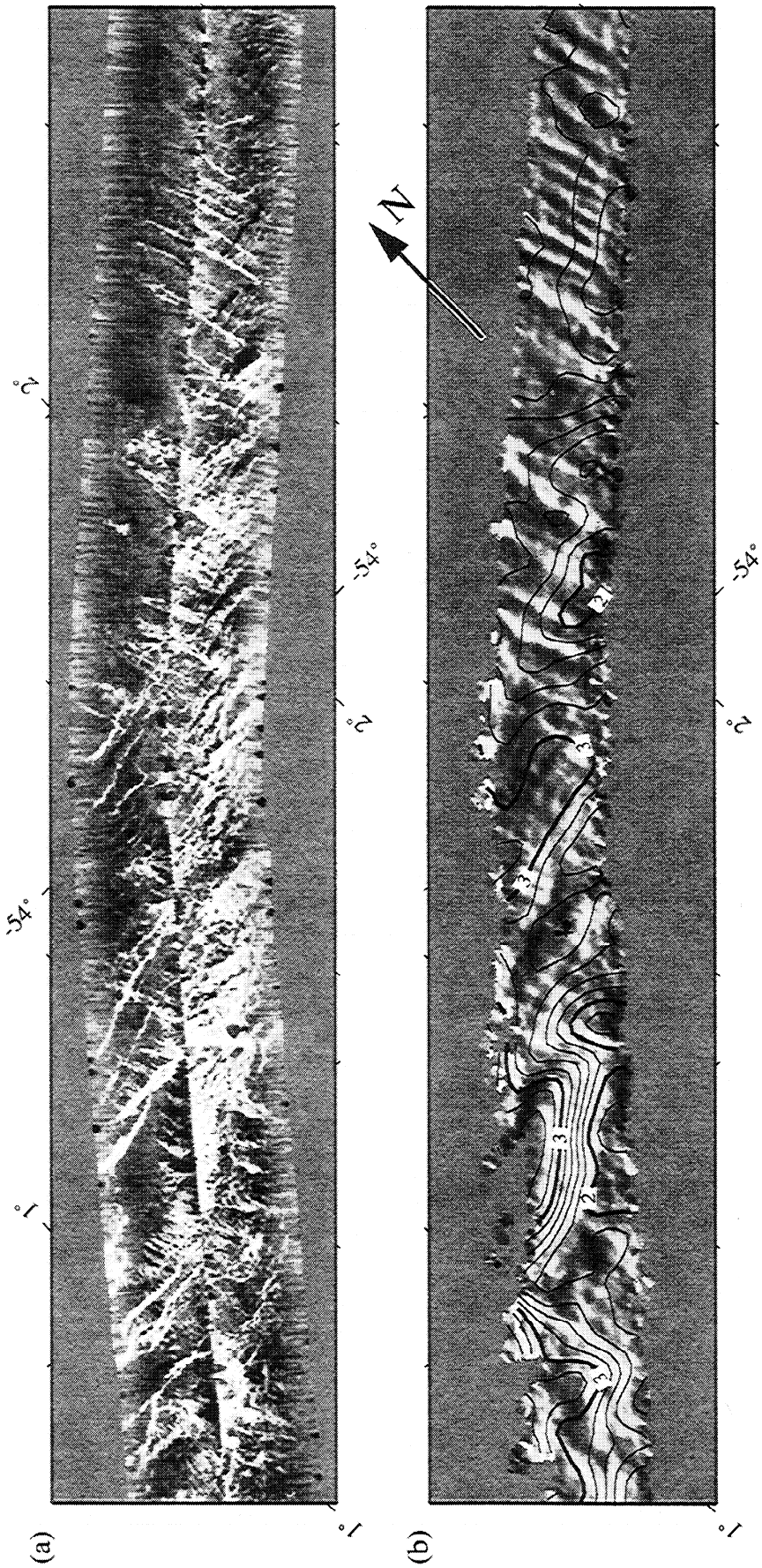


**Figure 4.** MR1 sonar data immediately northwest of the Bouvet transform valley showing (a) side-scan sonar image and (b) bathymetry with artificial illumination from the northwest. Annotation of contours is in kilometers. The image is an oblique Mercator projection with projection equator parallel to the Bouvet transform (azimuth 046°). Data processing is described by *Davis et al.* [1993].

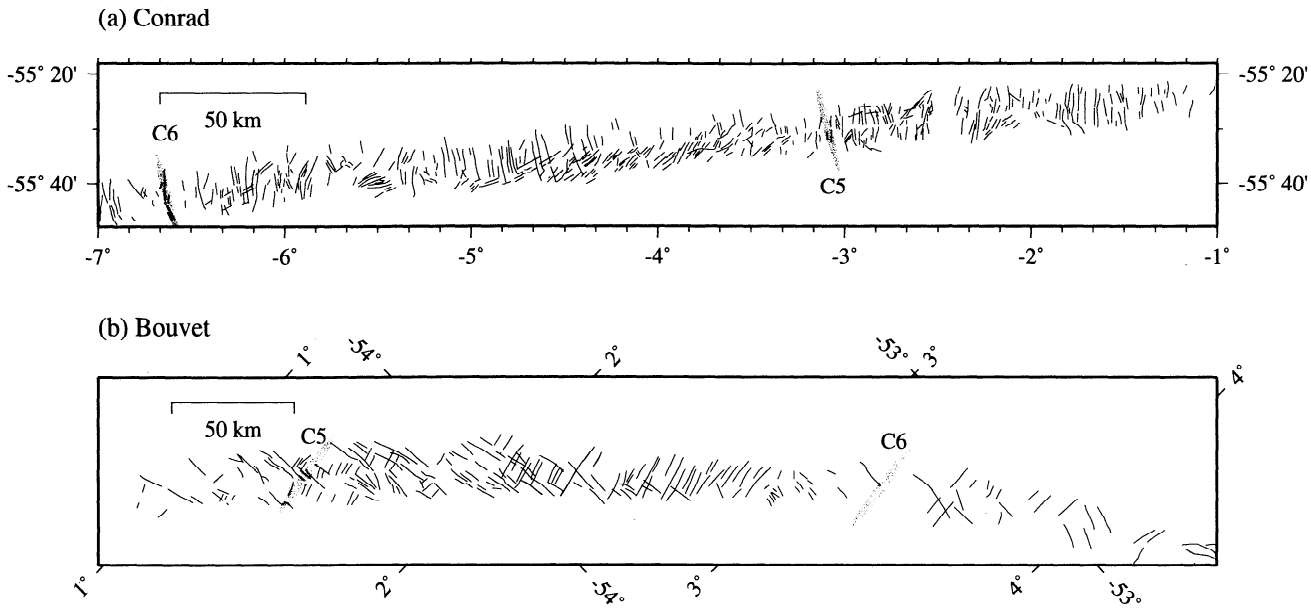


**Figure 5.** Interpreted lineaments adjacent to the (a) Conrad and (b) Bouvet transform. The shaded ellipses show our interpretations of chrons C5n.1n and C6n (young) in the magnetic anomalies.

interpret the disruption of reflectors along the basin center as the PTDZ, where strike-slip motion has juxtaposed different seismic facies. Southeast of the transform, oceanic basement is just visible beneath the sediments. The fanning of strata into the basin is undoubtedly due in part to differential compaction, although it probably also reflects extension across the transform. The upward folding of strata in the center may reflect brief periods of compression due to irregularities along the transform fault. Ephemeral compression would also explain the transform-parallel ridges along the valley floor in Figure 3. Near-surface reflectors are subhorizontal and onlap the underlying sequence, so recent deformation is almost exclusively strike-slip at the location of the seismic section.

Figure 8a shows an extensional basin immediately northwest of the transform valley (section C located in Figure 3b). The basin is a half-graben bounded by two main overlapping faults trending E-W and WNW-ESE, with a combined throw of ~1300 m. The basin sediments fan into the main faults, suggesting they were deposited during extension. Northward dipping reflectors in the half-graben footwall and elsewhere are probably due to out-of-plane scattering from SMAR fabrics.

At its northwest end, the seismic profile crosses one of the grabens forming the boundary of the deformation zone (Figure 9). The graben border faults disrupt the whole sedimentary sequence, suggesting that extension is recent. The northernmost fault of the section has a throw of approximately 700 m.

The seismic data, therefore, suggest a sequence of activity on the faults, and possibly a migration of extension from the transform valley and southeast area to the area northwest of the transform. The offset sediments in Figure 9 show that the faults are presently active or at least were recently active.

### 2.2. Hawaii-MR1 Sonar Data Adjacent to the Conrad Transform

An example of side-scan sonar images and bathymetry collected immediately north of the Conrad transform valley is shown in Figure 10, and Figure 5a shows interpreted lineaments. The west half of Figure 10 shows a SMAR fabric oriented slightly west of north. Further SMAR fabric occurs beyond the image (Figure 5). A second fabric runs southwest-northeast, mostly on the southern half of the swath, and coincides with prominent ridges in the bathymetry. These are probably tectonic features, with some scarps in the bathymetry facing southeast, although scarps are not obvious along some ridges so we cannot rule out a volcanic origin for some of them. Anomalous fabric orientations occur at 5°30'W (Figure 5), where we propose a ridge jump in the following section. Further unusual fabrics occur immediately east of 3°W, which is approximately where *Sclater et al.* [1976] proposed that the SMAR divided before evolving to the present configuration.

### 2.3. Magnetic Anomalies and Regional Bathymetry

Magnetic anomalies (Figures 11 and 12) were acquired along the ridges immediately north of the Conrad and Bouvet transforms (Figure 2b). They are typical large-amplitude marine anomalies, whose fidelity reflects the shallow depth to magnetic basement. In the following we model the profiles as though they were created along flow lines of plate motion (hence the data in Figures 11 and 12 are projected onto 070°), although, more strictly, they were created by a lengthening ridge adjacent to a southward migrating triple junction when it was in RFF mode. Figures 11 and 12 also show the anomalously shallow bathymetry adjacent to both transforms, which is typical of slow-spreading ridge transform valleys and their inactive extensions [*Collette*, 1986]. Within 100 km of the present ridge axes, the bathymetry is rugged reflecting the slow-spreading rates and volcanic construction adjacent to Spiess Ridge [*Mitchell and Livermore*, 1998b]. The shallow depths at -25 km in Figure 11, within 1500 m of sea level, correspond to the inside corner high of the Conrad transform with the easternmost segment of the SAAR [*Sclater et al.*, 1976]. Beyond 100 km in each case, the bathymetry is smoother, as expected for the faster-spreading SMAR, and

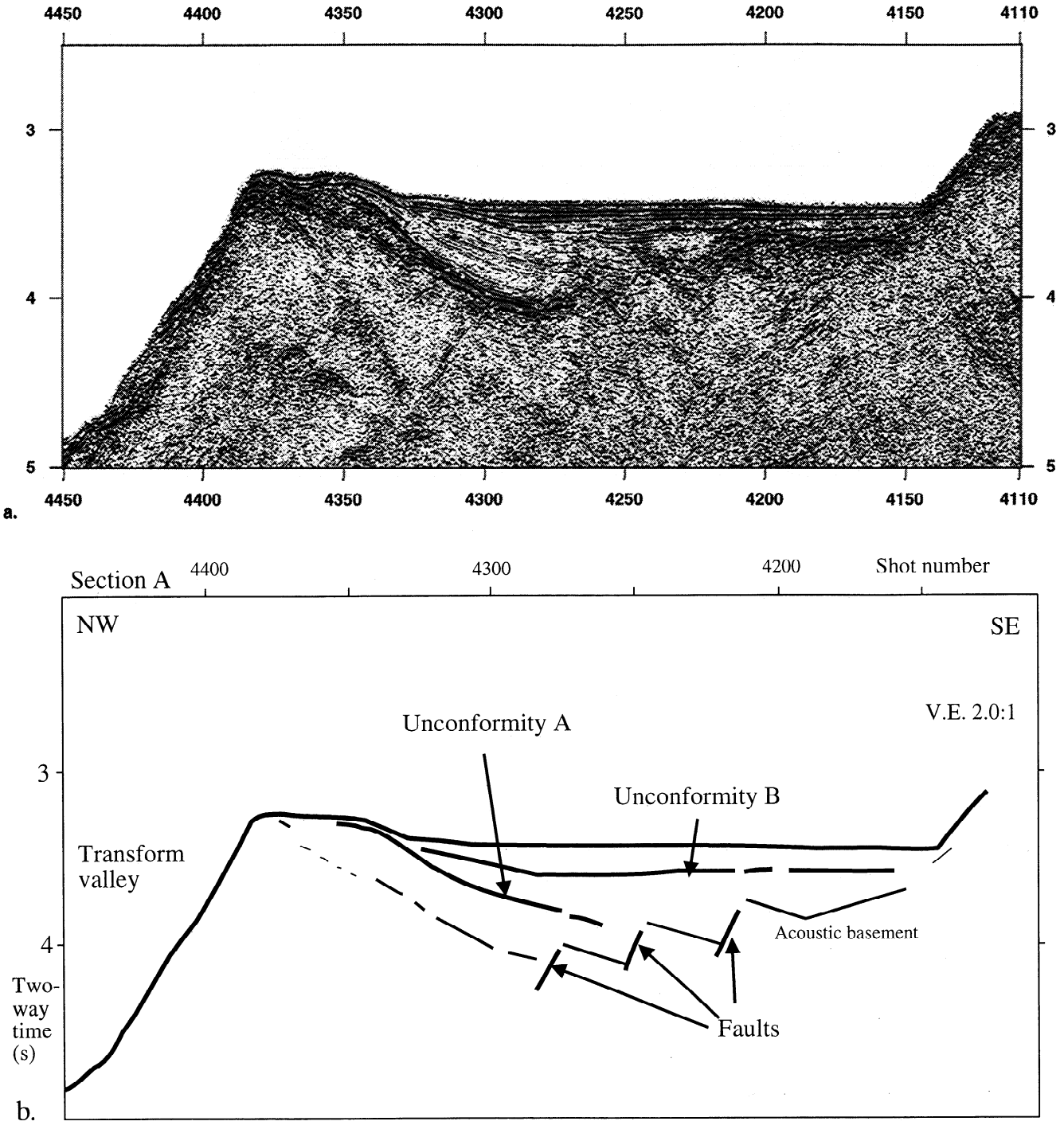


**Figure 6.** (a) This and Figures 7a, 8a, and 9a show sections of a 24-channel multichannel seismic line located in Figure 3b. Depth is given as seismic two-way time in seconds in this and Figures 7-9. Data were collected with a 25 m hydrophone group spacing and 50 m shot intervals (hence sixfold coverage). Processing was carried out at the Istituto di Geologia Marina in Bologna using the DISCO processing package of Cogniseis and included finite difference time migration. Numbers above profiles are shot numbers. (b) Interpretation of the seismic image showing two prominent unconformities. These imply a change in fault activity, with the two leftmost faults active while sediments below A were deposited, and the rightmost fault active while sediments below B were deposited. Vertical exaggeration (V.E.) here and in Figures 7b, 8b, and 9b relates to the seafloor profile assuming a water column velocity of 1500 m/s.

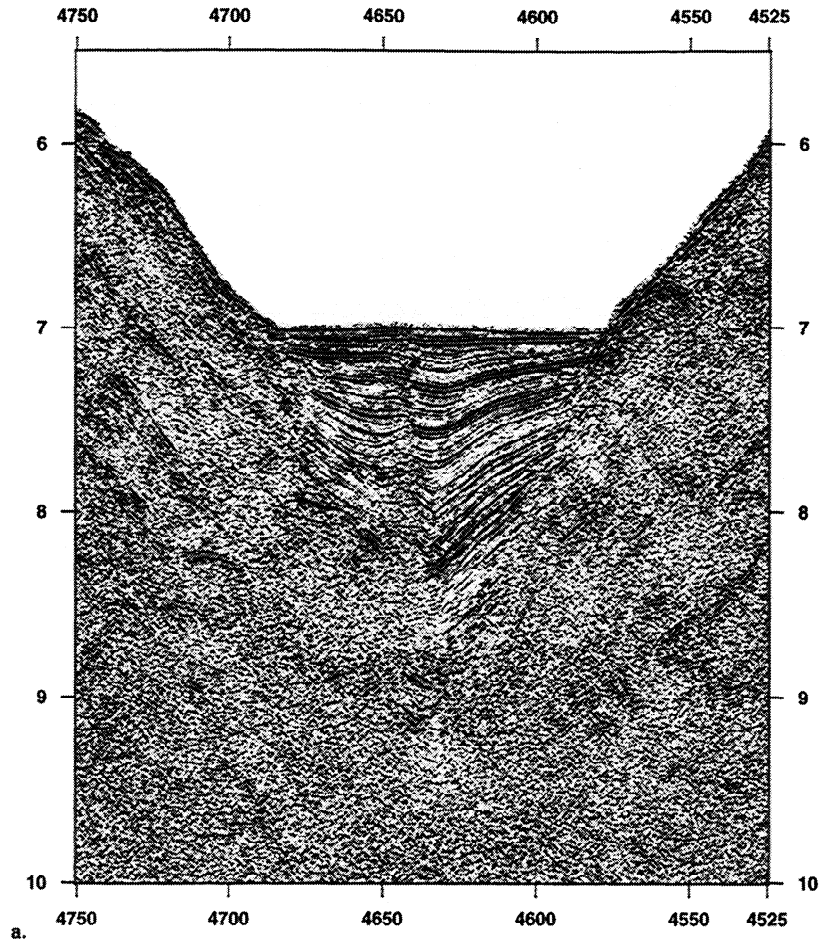


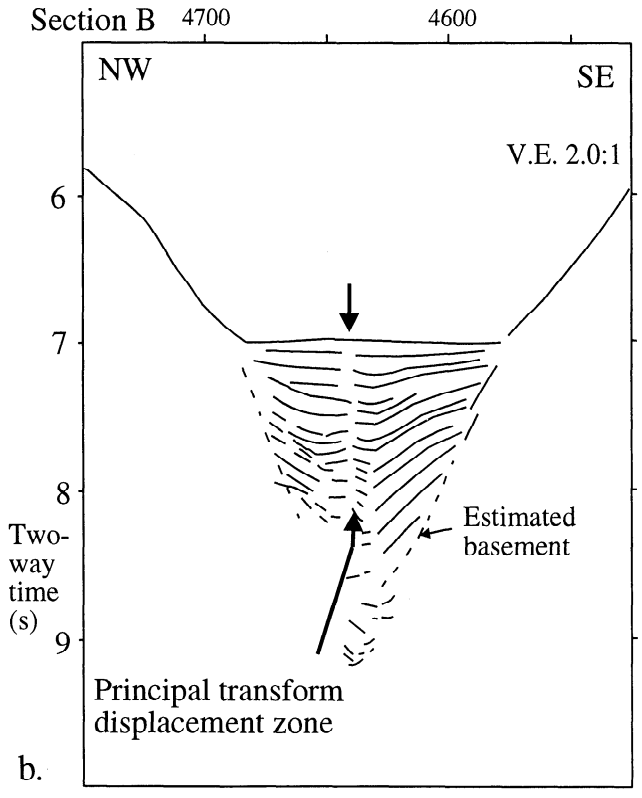


**Figure 7.** (a) Seismic image and (b) interpretation across the Bouvet transform valley (section B in Figure 3b). The disruption along the center marks the principal transform displacement zone. Sediment reflectors dip inward, possibly indicating extension across the transform valley.

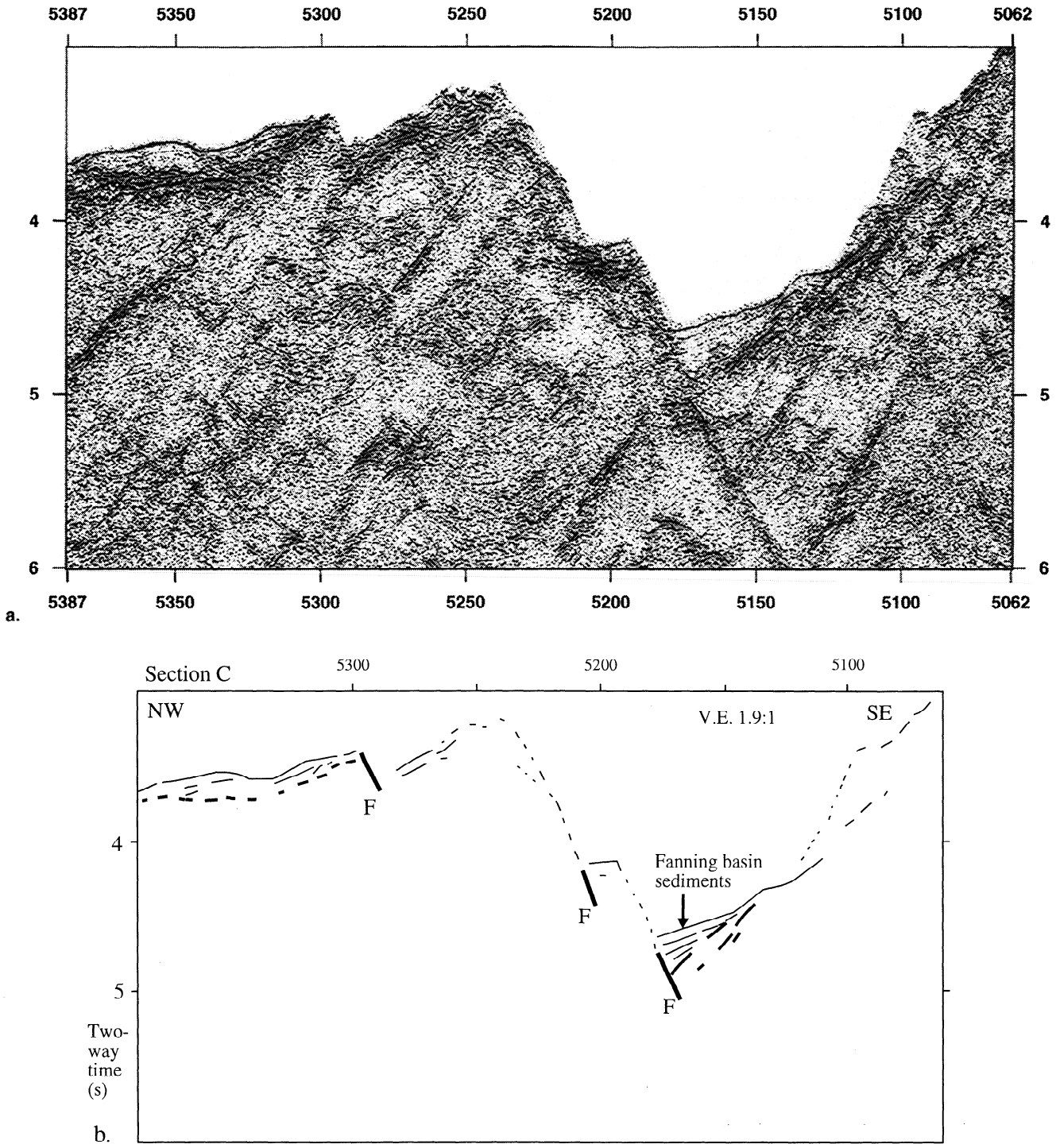


**Figure 8.** (a) Seismic image and (b) interpretation immediately northwest of the transform valley (section C in Figure 3b). The image shows a small basin with sloping sediments fanning into a fault scarp around shot point 5170, which may indicate sediments deposited during extension. Strong reflectors dipping to the left are probably due to out-of-plane scattering from SMAR abyssal hills.

follows a typical oceanic thermal subsidence trend [*Parsons and Sclater*, 1977], though with an initial depth 1 km shallower than normal.

Anomalies along both profiles were modeled using the polarity reversal timescale of *Cande and Kent* [1995], with only slight changes to spreading rates predicted by the SAM-AFR finite rotations of *Shaw and Cande* [1990]. Based on our attempts at modeling the anomalies, our best estimate of the time the triple junction stopped evolving as RFF is C5n.1n, so later anomalies were modeled using spreading rates appropriate for the SAAR and SWIR projected onto 070°. On the Conrad profile, good agreement with anomalies C1 to C2A was observed (Figure 11), but between 50 and 100 km west of the ridge axis, over a bathymetric trough separating the present inside corner high from

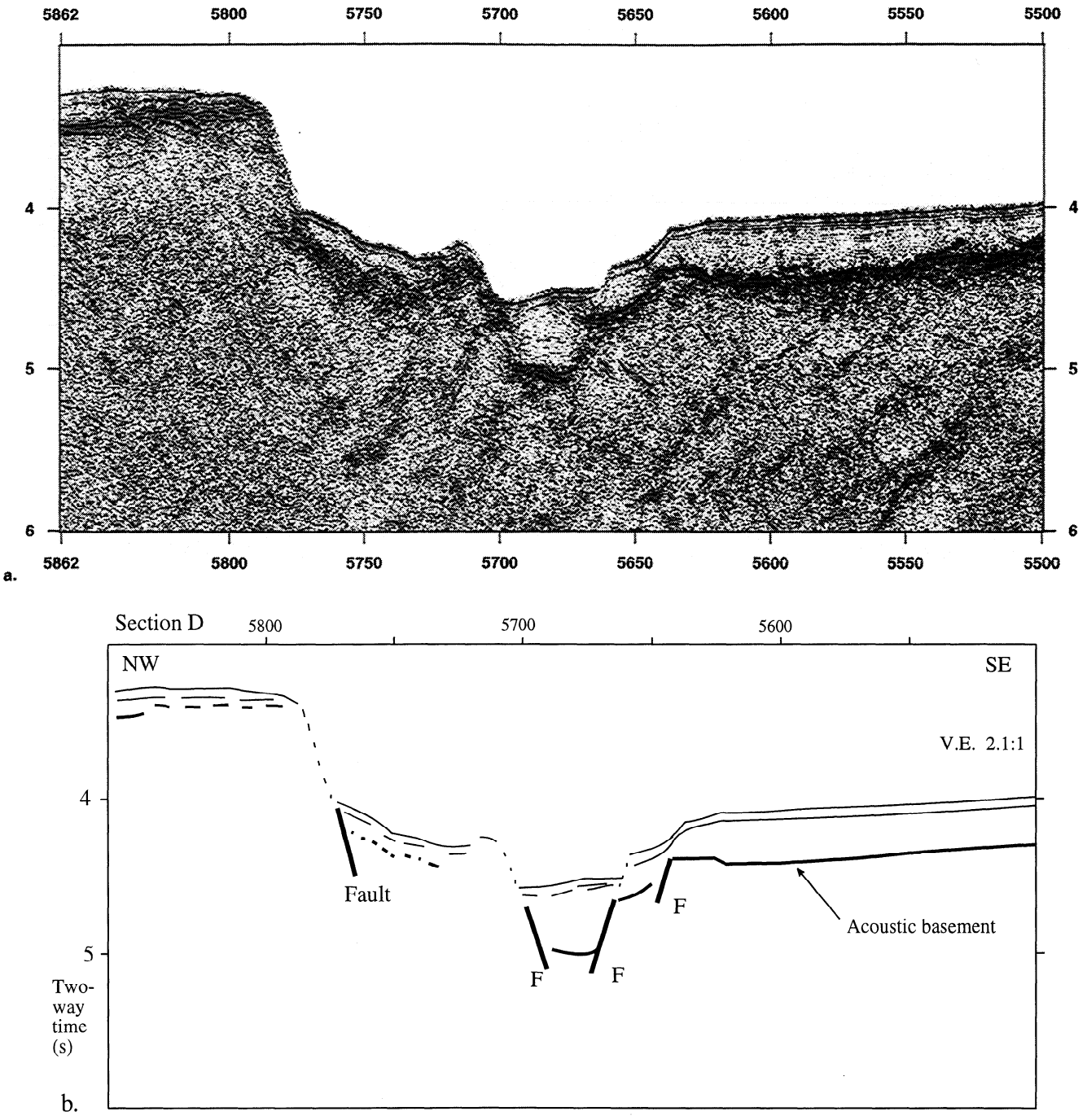


**Figure 9.** (a) Seismic image and (b) interpretation across the NW edge of the deformation zone (section D in Figure 3b). The image shows abrupt offsets of the sediment surface between shot points 5640 and 5680 which correspond to basement offsets and imply that faulting is recent.

the fracture zone ridge to the west, anomalies are not identifiable. Older anomalies are well formed but do not fit the model as well as the conjugate Bouvet anomalies. We are confident that anomalies C4 (8.07 Ma) to C5A (12.40 Ma) are present. We applied reconstruction poles [*Nankivell*, 1997; *Shaw and Cande*, 1990] to project C6 of the Bouvet side onto the Conrad side. Based on the projected location at around –320 to –330 km, we assigned C6 and C5E to the two large-amplitude anomalies at –300 km. Anomalies between C5E and C5A, however, are ambiguous and are not simply modeled with conjugate spreading rates to the Bouvet side.

We believe that the gap in the transform ridge near 5° 50'W (-250 km) represents a rift valley of an abandoned spreading center. The shallow dipping east side of the gap coincides with crenulations in the MR1 image which are transform-parallel. Their similarity to megamullions [*Tucholke et al.*, 1998] suggests they may represent a detachment fault formed during slowing extension rates associated with abandonment. Assuming that the

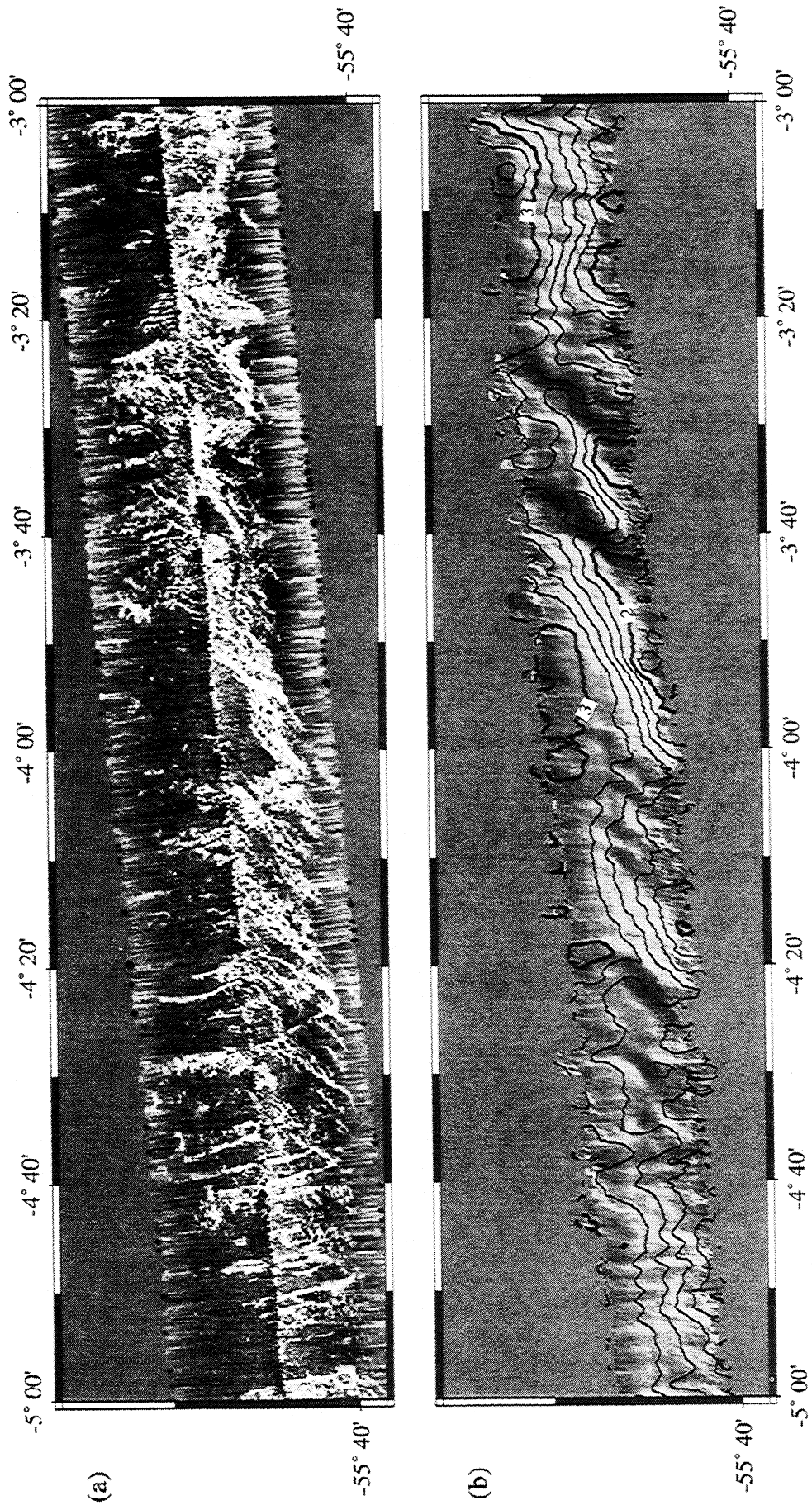


**Figure 10.** MR1 sonar data immediately north of the Conrad transform valley showing (a) side-scan sonar image and (b) bathymetry (Mercator projection) with artificial illumination from the northwest. Annotation of contours is in kilometers. Data processing is described by *Davis et al.* [1993].

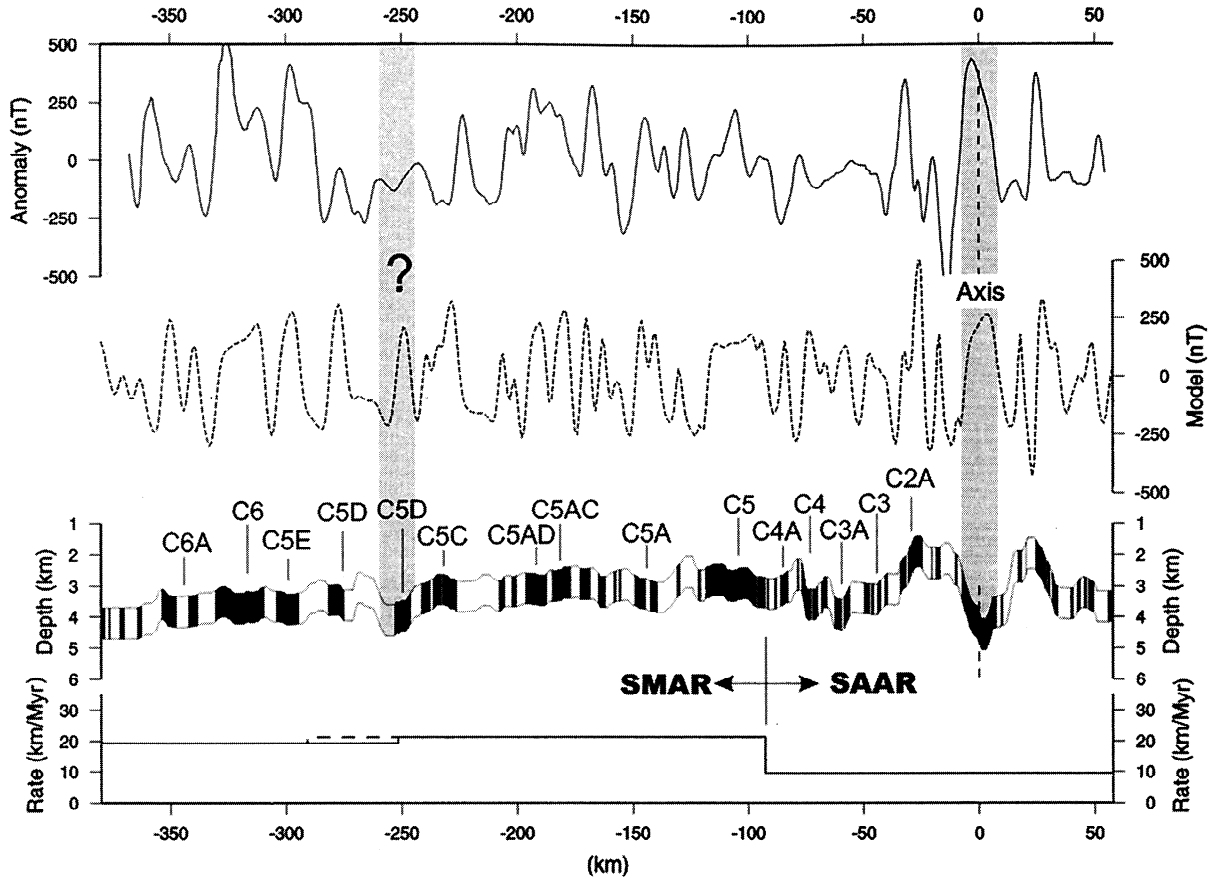


**Figure 11.** Magnetic anomaly model for data collected immediately north of the Conrad transform. The observed profile has been projected onto 070°E, the approximate direction of SAM-AFR motion. Dashes in the lower part of the figure show half-rates for SAM-AFR motion (from *Shaw and Cande* [1990]) and, after C5, for SAM-ANT (SAAR) motion projected onto 070°. The reversal timescale of *Cande and Kent* [1995] has been used to model the anomalies using a1 km thick source layer of susceptibility 0.06 and a smoothed version of the observed bathymetry. Anomalies associated with the present spreading center and with a postulated abandoned spreading center (marked with a question mark), are indicated.

large-amplitude anomalies at -300 km are C6 and C5E, the ridge would have been abandoned after the C5D normal polarity chron, leaving a C5D anomaly east of the fossil axis. The model in Figure 11 includes a 22 km eastward axis jump at 16.75 Ma (just before C5C).

On the Bouvet profile (Figure 12), an acceptable fit is obtained with a 22 km eastward ridge jump immediately following either chron C5E or chron C5D. We prefer the latter timing, which gives a jump identical to that modeled on the Conrad flank (hence C5D is omitted in Figure 12). The fit is remarkably good between anomalies C5 (9.74 Ma) and C6A (21.32 Ma). Beyond this, there is agreement back to C6B (23.07 Ma).

## 3. Fabric Orientations

We have used the lineament maps in Figure 5 to represent simple cross sections of the deformation zones and have analyzed the orientations of their structures. The lineament orientations are shown in Figure 13. On the Bouvet side, there are clearly two groups due to the SMAR fabrics and the crosscutting faults, which persist from 100 to 500 km. On the Conrad side, two groups are also seen, but they have more variable azimuth and the crosscutting fabrics only occur from -400 to -130 km. None of the groups show any clear systematic change in orientation with seafloor age, except for the fabrics immediately east of -150 km, which may have been created at the first segment of the SAAR and therefore have a SAAR trend. The change from SMAR to SAAR trends over -200 to -150 km could imply that the triple junction changed from RFF slightly later than chron C5, or it represents a period of spreading center reorientation.

Figure 14 shows distributions for a restricted range of the data in Figure 5, so that structures correspond to seafloor created at the SMAR of the proposed RFF triple junction (from C5 to a little beyond C6 seafloor). Figures 14a and 14b were computed by binning the data with a continuous weighting function [*Fisher*, 1993, eq. 2.2] with a 20° full width. These show narrow populations for the Bouvet side but more dispersed populations for the Conrad side. The continuous curves in Figures 14c and 14d show bimodal von Mises probability density functions (pdfs) [*Fisher*, 1993] fitted to the data. Their centroids are shown by the solid circles in Figures 14a and 14b, together with the present orientations (double-headed arrows) of the Bouvet and Conrad transforms measured from Figure 2b. The 68% widths of the pdfs are 41° and 24° for the Bouvet and 91° and 33° for the Conrad (crosscutting and SMAR fabrics, respectively). To provide a rough guide to the uncertainties, we varied the mode centroids with other model parameters fixed and defined the uncertainty region as that where total misfit is less than 10% of the typical

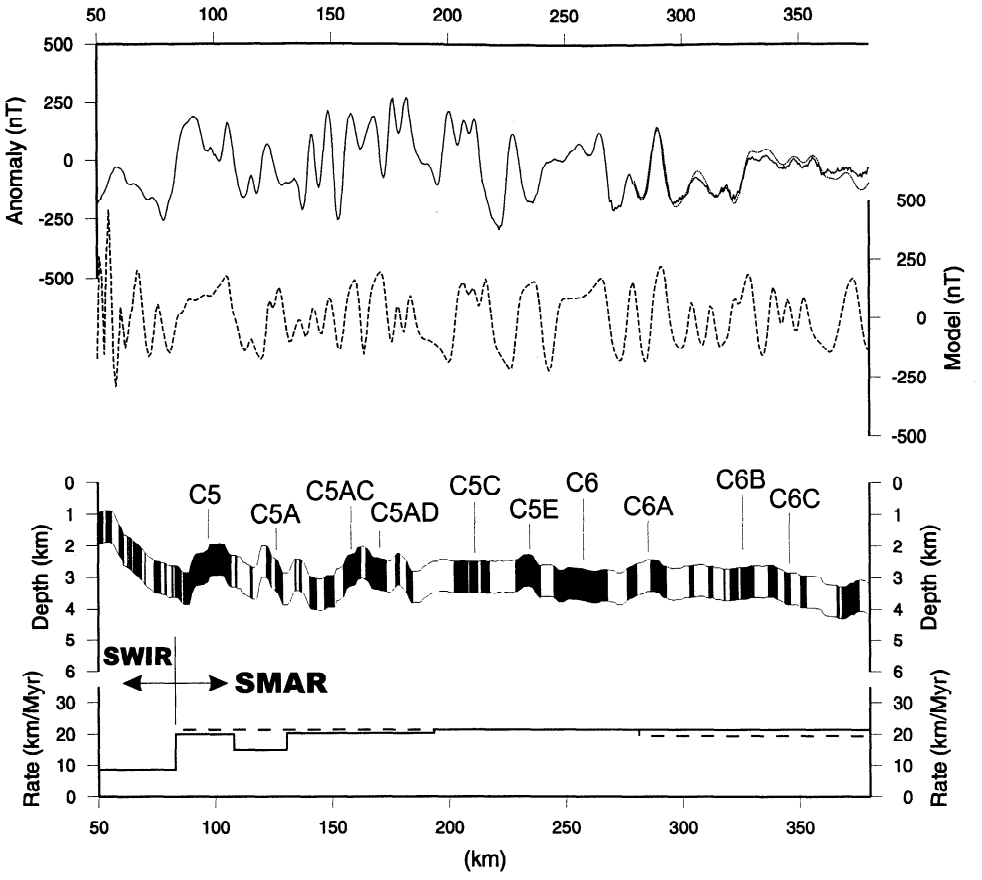


**Figure 12.** Magnetic anomaly model for data collected immediately north of the Bouvet transform. The observed profile has been projected onto 070°E, the approximate direction of SAM-AFR motion. Dashes in the lower part of the figure show half-rates for SAM-AFR motion (from *Shaw and Cande* [1990]) and, after C5, for SAM-ANT (SWIR) motion projected onto 070°. The reversal timescale and model parameters are as for Figure 11.

maximum value. These uncertainty estimates are ±9° and -2°/+3° for the modes in Figure 14c and ±5° and ±3° for the modes in Figure 14d (crosscutting and SMAR fabrics, respectively).

Figure 15a summarizes the modes of Figure 14 in the approximate configuration of the triple junction before chron C5. To estimate the effect of finite plate rotation, we rotated points on chron C5 and C6 South American and African seafloor onto Antarctica and derived average rotation angles for the C5-C6 period for each plate. We used the *Nankivell* [1997] plate reconstruction model, which was derived by a three-plate inversion of all existing South Atlantic anomaly identifications and provides the most accurate estimate of finite rotations. The Conrad and Bouvet modal orientations in Figure 15a have thus been adjusted by -1.3° and +2.8°, respectively. The dotted lines

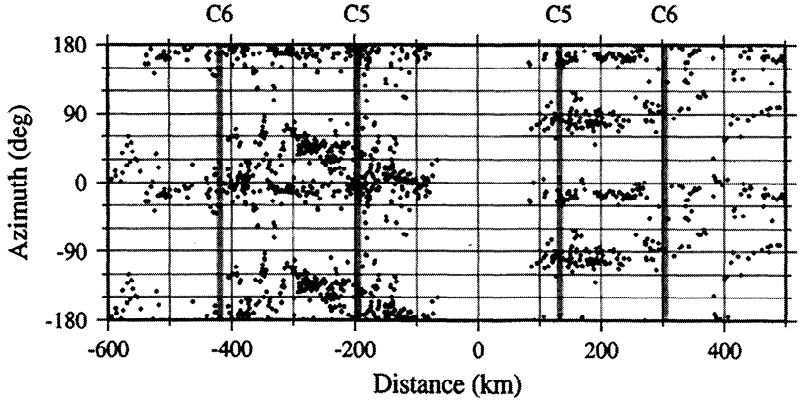


**Figure 13.** Lineament orientations with distance from the C5-C6 triple junction location (data are projected onto 048° (Bouvet) and 086° (Conrad) from an origin at 55°15'S, 0°00'E). The vertical shaded lines mark our interpretations of chrons C5n.1n and C6n in the magnetic anomalies.

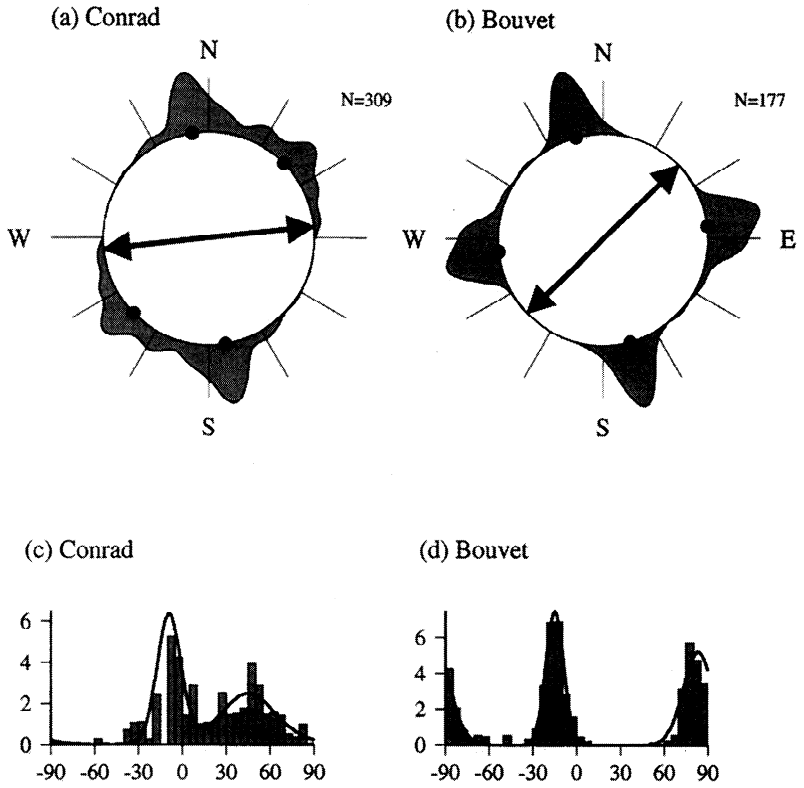


**Figure 14.** Orientation distributions for the lineaments in Figure 5 from 7° to 3.25°W (Conrad) and 1.3° to 3.7°E (Bouvet). (a and b) Distributions computed by binning the data with a continuous weighting function [*Fisher*, 1993, equation 2.2] with a 20° full width and with each value weighted by lineament length. The double-headed arrows show the present orientations of the Bouvet and Conrad transform valleys measured from Figure 2b. The solid circles show the modes located using the analysis in Figures 14c and 14d. (c and d) The continuous curves show bimodal von Mises probability density functions [*Fisher*, 1993] fitted to the binned data.

represent the dispersion of each mode (68% range), and shaded sectors represent the uncertainty in each mode's centroid. The SMAR fabrics north of the Bouvet transform are essentially parallel to those north of the Conrad transform (adjusted modes -12.2° and -10.4°, respectively), so, within observational error, the triple junction was probably RFF as suggested by *Sclater et al.* [1976] because a bifurcated SMAR or other non-RFF configuration would have probably created different fabric orientations on the two sides. The angles between the SMAR fabrics and their adjacent transforms are, however, quite different. The SMAR-Conrad angle is 84°, while the SMAR-Bouvet angle is 61°. The crosscutting fabrics approach the transforms at similar angles (42° for the Conrad and 37° for the Bouvet transform).

## 4. Transtensional Zone Interpretation

The faults crosscutting SMAR fabrics have similar orientations to tension gashes in shear zones [e.g., *Beach*, 1975], so we interpret them as normal faults due to transtensional deformation in zones parallel to the transforms (Figure 16a). To illustrate their geometry, if deformation involved plane wrench motion, the predicted initial fault orientations on the Bouvet side would be as shown in Figure 16b [*Wilcox et al.*, 1973]. T represents the orientations of tensional faults assumed to form perpendicular to the direction of maximum extensional strain, and R and R' are the Riedel and conjugate Riedel shear orientations. An alternative interpretation is that the faults initiated as Riedel shears and later developed normal slip displacements. Although we cannot rule out small strike-slip displacements based on these sonar data, initiation as Riedel shears is unlikely because they typically form at only 10°-30° to the wrench strike [*Wilcox et al.*, 1973; *Tchalenko*, 1970]. If faults had rotated from Riedel directions by bookshelf faulting [*Phipps Morgan and Kleinrock*, 1991], we would expect to observe significant clockwise rotation of SMAR fabrics within fault blocks and SMAR fabrics on SAM and AFR would not be parallel. Furthermore, we might expect development from Riedel shears to have left relicts of the original Riedel direction where normal displacements are small, which we do not observe. We therefore assume that the normal fault fabric simply initiated perpendicular to the direction of maximum extensional strain.

*McCoss* [1986] simplified the theory of transtensional zones [*Sanderson and Marchini*, 1984] to show that where displacement of the zone boundaries is not parallel to the zone, normal faults should initiate at an angle $\theta$ to the boundaries equal to half the angle of the displacement vector $A$ (Figure 16c). Hence, if deformation involves plane wrenching ($A$=90°), normal faults form with $\theta$=45°, and plane extension ($A$=0°) creates normal faults with $\theta$=0°. This simple relationship was derived by geometric arguments assuming that strain is continuous across an elongate deforming zone with rigid boundaries. Deformation is assumed to occur with constant volume so that (in this case) extension thins the crust but there is negligible volcanic intrusion, as suggested by the lack of later volcanic structures in the zone. From the modes of the crosscutting faults ($\theta$=42° and 37° for Conrad and Bouvet, respectively), the displacement vectors have

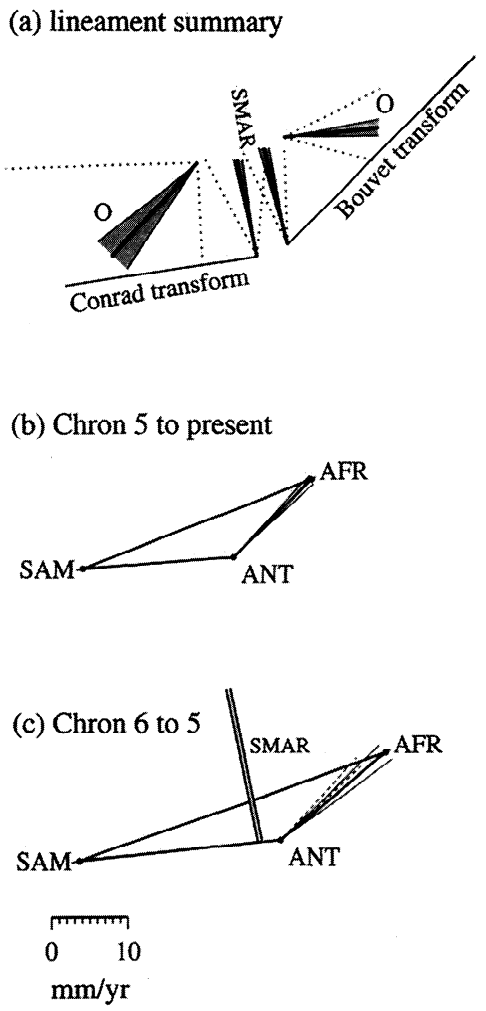


**Figure 15.** (a) Summary of the modes in Figure 14 with orientations adjusted for finite plate rotation (reconstructed to the present ANT reference frame) and plotted in the approximate configuration of the triple junction before chron C5. The dotted lines show the 68% range for each mode, and the shaded areas show the nominal uncertainty in the center of each mode. The SMAR fabrics north of the Bouvet and Conrad transforms are subparallel, confirming that the triple junction was probably RFF as suggested by *Sclater et al.* [1976]. (b) Velocity space diagram computed using the chron C5 reconstruction poles of *Nankivell* [1997]. (c) Velocity space diagram computed for fixed ANT using the chron C6 and C5 reconstruction poles of *Nankivell* [1997]. SMAR trend is drawn bisecting SAM-AFR with the average degree of asymmetric spreading derived from the magnetic anomalies (chrons C5n.1n to C6n (young)) and modal trend of fabrics in Figure 15a. The discrepancy with ANT velocity is discussed in the text. Both Figures 15b and 15c have the same velocity scale. Fine lines in Figures 15b and 15c show the 95% confidence interval in spreading directions for ANT-AFR predicted from the pole uncertainties of *Nankivell* [1997] (dashed lines in Figure 15c reproduce the uncertainty range from Figure 14c for comparison).

$A$=84° (Conrad) and $A$=74° (Bouvet), which correspond to a ratio of strike slip to divergence across the zones of between 3:1 and 10:1. Considering the uncertainties, the extensional component is poorly resolved, although $A$>90° is clearly ruled out because it would have produced compression. The divergence is also underestimated on the Bouvet side because we have not accounted for the grabens along the northwest of the zone. Since we cannot rule out minor bookshelf-type rotations of the faults, θ will slightly overestimate the original fault orientation, and hence this also leads to an underestimate of the extensional component. The deformation is "divergent strike slip" in the classification of *Krantz* [1995], that is, wrenching with minor extension.

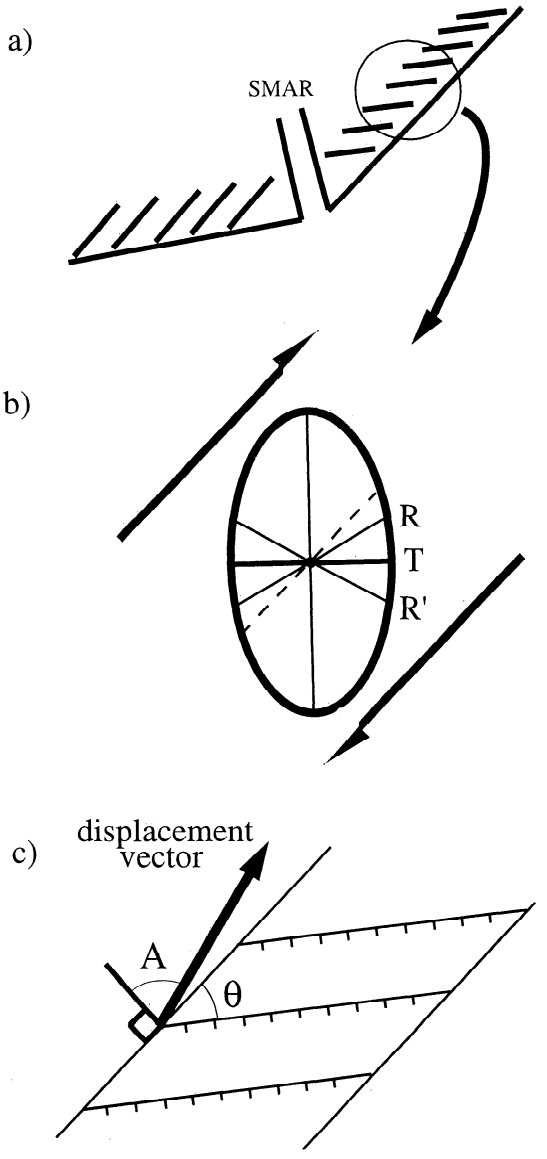


**Figure 16.** Interpretation of the regions of crosscutting faults as transtensional zones. (a) Configuration of the deformation zones adjacent to the Bouvet and Conrad transforms. (b) Strain ellipse and associated fault trends [*Wilcox et al.*, 1973] for plane wrenching across an elongate shear zone. T represents the initial orientation of tensional faults formed perpendicular to the direction of maximum extensional strain. R and R' are the Riedel and conjugate Riedel shear trends. (c) If displacement across the zone is not parallel to the zone boundaries, deformation is transtensional. Assuming that normal faults initiated perpendicular to the direction of maximum extensional strain and have not greatly rotated, the vector representing net displacement across the zone has an orientation given by the angle $A=2\theta$ [*McCoss*, 1986]. For the Bouvet and Conrad transforms, θ is 37° and 42° so $A$ is 74° and 84°, respectively (i.e., with minor divergence compared to the wrenching).

This deformation probably reflects only a small displacement of the zone boundaries compared to the plate velocities. From the vertical relief on normal faults along the seismic line marked in Figure 3b (total 4.2 km outside the Bouvet transform valley) and assuming that rotation of faults about horizontal axes is small and 45° fault dips typical of normal-faulting oceanic earthquakes [*Solomon et al.*, 1988], the net extension may be no more than 4 km. This corresponds to a displacement rate of only 0.3 mm/yr averaged over the 13 Myr life of the seafloor here. Because the extension intensifies toward the southwest corner of the African plate (Figure 3a), the Bouvet PTDZ is not necessarily parallel to AFR-ANT motion, and the fact that the PTDZ lies 4°-5° anticlockwise from AFR-ANT in the NUVEL-1A plate model [*DeMets et al.*, 1994] would be consistent with 0.9-1.2 mm/yr greater extension to the southwest. However, we observe no evidence for a conjugate deformation zone on the Antarctic plate where the Bouvet transform intersects the first SWIR segment at 3°E, and the accuracy of the NUVEL-1A model precludes a discussion of plate kinematics at this scale.

## 5. Discussion

### 5.1. Southernmost Mid-Atlantic Ridge Structure

The SMAR probably had a normal axial structure because we observe typical fabrics with a narrow range of orientations (Figures 5-15) and magnetic anomalies have high fidelity (Figures 11 and 12). During RFF mode the SMAR would have had the unusual structure of two back-to-back ridge-transform intersections, so we were curious to see if there were indications of any unusual crustal structure. The tectonic and magnetic structure is not obviously unusual, and in particular we found no evidence for large-slip, low-angle normal faults proposed elsewhere for areas adjacent to other Mid-Atlantic Ridge transforms [*Cann et al.*, 1997; *Tucholke et al.*, 1998; *Mitchell et al.*, 1998] (except at 55° 40'S, 5° 30'W, possibly associated with a ridge jump). The thermal structure of the triple junction would have been unusual, however. While normal ridge-transform intersections (RTIs) have cold old lithosphere sliding past the active ridge, with young lithosphere reheating the old lithosphere, at the Bouvet RFF triple junction the SMAR would have been almost stationary relative to the Antarctic plate to the south for ~10 Ma, significant compared to the adjacent Antarctic seafloor age 0-10 Ma during this time interval if the transforms grew from zero offset [*Sclater et al.*, 1976]. *Rutter and Brodie* [1987] proposed that thermal dehydration of serpentinite by the young lithosphere in oceanic transforms creates shear zones lined with ultrafine-grained olivine and dramatic weakening. If correct, this mechanism would be less important around RFF triple junctions because the old lithosphere may already be dehydrated, leading to higher transform resistance and providing a further explanation for the transtensional deformation discussed below.

### 5.2. Orientation of the Southernmost Mid-Atlantic Ridge

Figure 15a shows that the Conrad and Bouvet transform orientations are consistent with SAM-ANT and AFR-ANT motions (Figures 15b and 15c) predicted from plate reconstruction poles [*Nankivell*, 1997], which therefore accurately predict the plate velocities here. (The small discrepancy for the Conrad transform between Figures 15a and 15b reflects the short length of plate boundary magnetic anomalies available to constrain its spreading history.) The orientation of SMAR fabrics (Figure 15c), however, is 7° clockwise from the SAM-AFR normal and is difficult to explain by errors in the plate velocities (a greater northward SAM velocity component of 5 mm/yr would be difficult to justify because of the Conrad transform valley orientation). The SMAR normal trend expected from the AFR-SAM plate velocity (Figure 15c) and the measured modal orientation (from Figure 14b) are shown in the top right of Figure 3a. Away from the transform valley, fabric trends are normal, but close to the transform valley, SMAR trends are more variable and centered on this 7° oblique trend. Furthermore, C5 and C6 marked in Figure 2b with these SMAR trends are also not parallel to normal Mid-Atlantic Ridge abyssal hill trends observed in the gravity data northwest of the triple junction. Since there is little evidence for significant block rotation about vertical axes (in particular, SMAR fabrics are parallel on AFR and SAM), this 7° obliquity is probably original.

At ridge-transform intersections not involving triple junctions, the axial neovolcanic zone and ridge-parallel normal faults curve toward the transform valley. *Phipps Morgan and Parmentier* [1984] attributed this to a change in orientation of the horizontal principal stresses caused by resistance on the adjacent transform fault. We interpret the oblique SMAR at the Bouvet RFF triple junction as due to a competition between the effects of the Bouvet and Conrad transforms, while variability of SMAR orientations reflects fluctuating resistance on the two transforms. Since the SMAR was oriented clockwise, resistance was greatest along the Conrad transform. The origin of this is unclear, but we speculate that if the Bouvet transform extension started significantly prior to C5, reduced normal stress on the transform fault might have affected frictional resistance.

### 5.3. SMAR Drift With Respect to Antarctica

The SMAR trend in Figure 15c bisects SAM-AFR, with the degree of asymmetry deduced from the magnetic anomalies (C5n.1n to C6n (young)). The SMAR line does not intersect ANT, suggesting that the ridge drifted westward with respect to ANT by a little less than 3 mm/yr. This is a small effect compared to uncertainties in SMAR spreading asymmetry and plate velocities, but it would be difficult to accommodate in a rigid plate velocity analysis [*McKenzie and Morgan*, 1969] if transform boundaries are required to occur along the ANT-AFR and SAM-ANT vectors. (It is less problematic, however, if the plates are not required to be perfectly rigid [*Mitchell*, 1991].) The westward SMAR drift relative to ANT amounts to less than 30 km over 10 Myr and would have been accompanied by north-south adjustments of the transform faults by less than half this distance, a relatively small effect, though possibly affecting the peculiar deformation discussed below.

### 5.4. Transtensional Deformation

Oceanic transtensional zones of the extent found here are uncommon. Extensional transforms with extensive volcanism ("leaky transforms") and oblique spreading centers form a continuous set of plate boundaries with varying degrees of obliquity [*Taylor et al.*, 1994; *Tuckwell et al.*, 1996]. The transtensional zones found here are different, however, because deformation occurred over a broad area outside the plate boundary. We know of only one comparable example adjacent to the Willaumez tranform fault in the Manus Basin [*Taylor et al.*, 1994]. Transtensional normal faults lie adjacent to the Clipperton transform [*Pockalny*, 1997] but cover a limited area. Small faults

lying at 15° to the Charlie Gibbs transform are probably Riedel shears [*Searle*, 1981]. Curvature of fabrics adjacent to the Bullard transform (which are also crossed by Riedel-like structures) suggests they were deformed by strike-slip reactivation of ridge axis normal faults by bookshelf faulting [*Livermore et al.*, 1991], although otherwise this zone has comparable area to the Bouvet zone. Regions between overlapping spreading centers are potentially sites of transtensional deformation. The largest is 100 km across involving seafloor up to 1 Ma [*Hey et al.*, 1995], but it and other such regions appear to deform by "bookshelf" faulting [*Kleinrock and Hey*, 1989; *Phipps Morgan and Kleinrock*, 1991; *Wetzel et al.*, 1993].

Why the deformation lies outside the plate boundary is unclear. Seismic studies and dredging suggest that seafloor in transform valleys is extensively fractured and contains substantial serpentinite [e.g., *White et al.*, 1985]. Owing to the fracturing and the weak rheology of serpentinite, deformation due to plate motion changes commonly occurs within transform valleys rather than in their surrounding plates [e.g., *Tucholke and Schouten*, 1989]. Weakening of the lithosphere due to a hotspot under Bouvet Island or Spiess Ridge may explain why the deformation is locally intense immediately east of Spiess Ridge. Although the rheologies are clearly different, it would be interesting to explore whether high heat flow and thin brittle lithosphere could lead to widespread deformation in a similar way to that described for Basin and Range rifting, where cooling under slow extension offsets tectonic thinning, causing deformation to broaden [e.g., *Buck*, 1991].

The origin of the extensional component is also unclear. We suspect that plate motion changes are not the main or sole cause because further side-scan sonar and multibeam bathymetry of other transforms along the SAAR and SWIR do not show transtensional deformation of this extent [*Dick et al.*, 1991; *Livermore et al.*, 1991; also N. Grindlay personal communication; cruise JR9a unpublished data, 1995]. Figures 15b and 15c show velocity space diagrams for chron C5 to present and C6 to C5, computed from the poles of *Nankivell* [1997]. Although the poles suggest a change in the direction of AFR-ANT motion, the change is not significant (95% confidence intervals shown by the fine lines in Figures 15b and 15c). However, the total amount of transform-normal extension required to form the normal faults in Figure 3a is small, as explained earlier, so extension is not precluded by the plate motions.

An alternative possibility might be that extension arises because of the triple junction geometry. Considered in the ANT reference frame, SAM is moving to the west, and AFR is moving to the northeast. If stresses within the plates are aligned with this motion far from the boundaries, the north component of the African plate stress is balanced by tension along the plate boundaries, predicting extension across the transforms. This is highly speculative because traction by the underlying asthenosphere also influences stress state in an unknown way but we suggest that the origin of the deformation is probably local because widespread deformation is not found elsewhere along the plate boundaries.

## 6. Conclusions

The MR1 and Simrad EM12 sonar data show that SMAR fabrics on C5-C6 seafloor adjacent to the Bouvet and Conrad transforms are parallel to each other, so they were most likely formed at the same ridge and the triple junction was RFF. The exact time the triple junction started in RFF is unclear from our magnetic anomaly data, although chron C6 [*Sclater et al.*, 1976] would be reasonable, while a decrease in spreading rate and change in fabric orientations suggests that the RFF mode ended at around chron C5n.1n (~10 Ma) or shortly thereafter. SMAR fabrics are oriented 7° clockwise from their trends expected from AFR-SAM motion predicted from plate reconstruction poles, so the ridge was spreading slightly obliquely. By analogy with obliquely oriented fabrics at ridge-transform intersections elsewhere, we speculate that SMAR obliquity is due to competition between traction on the two transforms, the sense of obliquity here implying greater traction on the Conrad transform.

Seafloor adjacent to the transform valleys shows transtensional deformation, especially intense on the Bouvet side. A geometric analysis suggests that the deformation occurred with a ratio of strike slip to extension of 3:1 to 10:1. This is an inaccurate value because of variability of fault azimuths and because we assume that fabrics have not been greatly rotated (rotation and unaccounted normal faults mean that the extensional component is underestimated). The deformation is divergent strike slip in the classification of *Krantz* [1995]. Seismic data across the Bouvet transform show that the deformation is ongoing and may have progressively concentrated toward the northwest there. Since deformation of this extent is not generally found elsewhere along the SWIR plate boundary, it probably has a local origin. Speculative explanations include (1) local weakening of the lithosphere by the Spiess-Bouvet hotspot, (2) anomalously high traction along the transform faults, (3) tensional stresses along the transforms resulting from the three-way divergence of the plates around the triple junction, (4) shearing caused by westward movement of the southernmost Mid-Atlantic Ridge with respect to ANT (because the SMAR does not intersect ANT in the velocity triangle) and consequent realignment of transform faults, and (5) unresolved plate motion changes. Explanation 1 may be tested by studying the structure of other transforms close to plumes, while explanations 4 and 5 may be resolved as the accuracy of plate models improves. However, further surveying of RFF triple junctions and their ancient traces left on the plates will be needed to see if these structures are common and therefore if processes peculiar to triple junctions give rise to this kind of deformation.

**Acknowledgments.** We thank the officers and crews of RRS *James Clark Ross*, R/V *Gelendzhik* and R/V *Strakhov* for help in collecting the data presented here. Enrico Bonatti, Marco Ligi, Hans Schenke, and Rick Hagen are thanked for providing copies of multibeam data for survey planning, while Philippe Patriat, Sang-Mook Lee, and two anonymous reviewers are thanked for helpful comments. The Hawaii-MR1 system and data processing were provided by the University of Hawaii (J.R. Erickson, F. Martinez, L.D. Petersen, and D.D. Joseph). Some figures in this paper were produced with the GMT system [*Wessel and Smith*, 1991]. The seismic and Simrad data shown here were collected on surveys of the *Gelendzhik* and *Strakhov* funded by the CNR, Italy, and initiated by Marco Ligi and Enrico Bonatti. This work was supported by the Natural Environment Research Council (grants GR3/8900 and GT5/92/GS/5) and by a Royal Society University Research Fellowship (N.C.M.).

## References

Apotria, T. G., and N. H. Gray, Absolute motion and evolution of the Bouvet triple tunction, *Nature, 316*, 623-625, 1985.

Barker, P. F., and L. A. Lawver, South American - Antarctic plate motion over the past 50 Ma, and the evolution of the South American - Antarctic Ridge, *Geophys. J. R. Astron. Soc., 94*, 377-386, 1988.

Beach, A., The geometry of en-echelon vein arrays, *Tectonophyics., 28*, 245-263, 1975.

Bonatti, E., M. Ligi, L. Gasperini, A. Peyve, Y. Raznitsin, and Y. J. Chen, Transform migration and vertical tectonics at the Romanche fracture zone, equatorial Atlantic, *J. Geophys. Res., 99,* 21,779-21,802, 1994.

Buck, W. R., Modes of continental lithospheric extension, *J. Geophys. Res., 96,* 20,161-20,178, 1991.

Cande, S.C., and D.V. Kent, Revised calibration of the geomagnetic polarity timescale for the late Cretaceous and Cenozoic, *J. Geophys. Res., 100,* 6093-6095, 1995.

Cann, J. R., D. K. Blackman, D. K. Smith, E. McAllister, B. Janssen, S. Mello, E. Avgerinos, A. R. Pascoe, and J. Escartin, Corrugated slip surfaces formed at ridge-transform intersections on the Mid-Atlantic Ridge, *Nature, 385,* 329-332, 1997.

Collette, B.J., Fracture zones of the North Atlantic: Morphology and a model, *J. Geol. Soc. London, 143,* 763-774, 1986.

Davis, R., S. Zisk, M. Simpson, M. Edwards, A. Shor, and E. Halter, Hawaii mapping research group bathymetric and sidescan processing, paper presented at *Oceans '93,* Inst. of Electr. and Electron. Eng., New York, 1993.

DeMets, C., R. G. Gordon, D. F. Argus, and S. Stein, Effect of recent revisions to the geomagnetic reversal timescale on estimates of current plate motions, *Geophys. Res. Lett., 21,* 2191-2194, 1994.

Dick, H. J. B., H. Schouten, P. S. Meyer, D. G. Gallo, H. Bergh, R. Tyce, P. Patriat, K. T. M. Johnson, J. Snow, and A. Fisher, Tectonic evolution of the Atlantis II fracture zone, in *Proc. Ocean Drilling Program, Sci. Res. 118,* edited by R. P. Von Herzen and P. T. Robinson, pp. 359-398, Ocean Drilling Program, College Station, Tex., 1991.

Dziewonski, A. M., and J. H. Woodhouse, An experiment in systematic study of global seismicity - centroid-moment tensor solutions for 201 moderate and large earthquakes of 1981, *J. Geophys. Res., 88,* 3247-3271, 1983.

Dziewonski, A. M., T. A. Chou, and J. H. Woodhouse, Determination of earthquake source parameters from waveform data for studies of global and regional seismicity, *J. Geophys. Res., 86,* 2825-2852, 1981.

Fisher, N. I., *Statistical Analysis of Circular Data,* 277 pp., Cambridge Univ. Press, New York, 1993.

Forsyth, D. W., Fault plane solutions and tectonics of the South Atlantic and Scotia Sea, *J. Geophys. Res., 80,* 1429-1443, 1975.

Hey, R. N., P. D. Johnson, F. Martinez, J. Korenaga, M. L. Somers, Q. J. Huggett, T. P. LeBas, R. I. Rusby, and D. F. Naar, Plate boundary reorganization at a large-offset, rapidly propagating rift, *Nature, 378,* 167-170, 1995.

Johnson, G. L., R. N. Hey, and A. Lowrie, Marine geology in the environs of Bouvet Island and the South Atlantic triple junction, *Mar. Geophys. Res., 2,* 23-36, 1973.

Kleinrock, M.C., and R.N. Hey, Migrating transform zone and lithospheric transfer at the Galapagos 95.5°W propagator, *J. Geophys. Res., 94,* 13,859-13,878, 1989.

Kleinrock, M. C., and J. Phipps Morgan, Triple junction reorganization, *J. Geophys. Res., 93,* 2981-2996, 1988.

Krantz, R. W., The transpressional strain model applied to strike-slip, oblique-convergent and oblique-divergent deformation, *J. Struct. Geol., 17,* 1125-1137, 1995.

Lawver, L. A., J. G. Sclater, and L. Menke, Mesozoic and Cenozoic reconstructions of the South Atlantic, *Tectonophyics., 114,* 233-254, 1985.

Ligi, M., E. Bonatti, G. Bortoluzzi, G. Carrara, P. Fabretti, D. Penitenti, D. Gilod, A. A. Peyve, S. Skolotnev, and N. Turko, Death and transfiguration of a triple junction in the South Atlantic, *Science, 276,* 243-245, 1997.

Livermore, R. A., J. S. Tomlinson, and R. W. Woollett, Unusual sea-floor fabric near the Bullard fracture zone imaged by GLORIA sidescan sonar, *Nature, 353,* 158-161, 1991.

McCoss, A. M., Simple constructions for deformation in transpression/transtension zones, *J. Struct. Geol., 8,* 715-718, 1986.

McKenzie, D. P., and W. J. Morgan, Evolution of triple junctions, *Nature, 224,* 125-133, 1969.

Mitchell, N. C., Distributed extension at the Indian Ocean triple junction, *J. Geophys. Res., 96,* 8019-8043, 1991.

Mitchell, N. C., and R. A. Livermore, The present configuration of the Bouvet triple junction, *Geology, 26,* 267-270, 1998a.

Mitchell, N. C., and R. A. Livermore, Spiess Ridge: An axial high on the slow-spreading Southwest Indian Ridge, *J. Geophys. Res., 103,* 15457-15471, 1998b.

Mitchell, N. C., J. Escartin, and S. Allerton, Detachment faults at mid-ocean ridges garner interest, *Eos, Trans. AGU, 79,* 127, 1998.

Nankivell, A., Tectonic Evolution of the Southern Oceans, D. Phil. thesis, 303 pp., Univ. of Oxford, Oxford, England, 1997.

Parsons, B., and J. G. Sclater, An analysis of the variation of ocean floor bathymetry and heat flow with age, *J. Geophys. Res., 82,* 803-827, 1977.

Patriat, P., and P. Courtillot, On the stability of triple junctions and its relation to episodicity in spreading, *Tectonics, 3,* 317-332, 1984.

Phipps Morgan, J., and M. C. Kleinrock, Transform zone migration: Implications of bookshelf faulting at oceanic and Icelandic propagating ridges, *Tectonics, 10,* 920-935, 1991.

Phipps Morgan, J., and E. M. Parmentier, Lithospheric stress near a ridge-transform intersection, *Geophys. Res. Lett., 11,* 113-116, 1984.

Pockalny, R. A., Evidence of transpression along the Clipperton transform: Implications for processes of plate boundary reorganization, *Earth Planet. Sci. Lett., 146,* 449-464, 1997.

Rognstad, M., Hawaii MR1: A new underwater mapping tool, in *Proceedings of the International Conference on Signal Processing and Technology,* pp. 900-905, DSP Assoc., Newton, Mass., 1992.

Rutter, E. H., and K. H. Brodie, On the mechanical properties of oceanic transform faults, *Ann. Tecton., 1,* 87-96, 1987.

Sanderson, D. J., and W. R. D. Marchini, Transpression, *J. Struct. Geol., 6,* 449-458, 1984.

Sandwell, D. T., and W. H. F. Smith, Marine gravity anomaly from Geosat and ERS-1 satellite altimetry, *J. Geophys. Res., 102,* 10,039-10,054, 1997.

Sclater, J. G., C. Bowin, R. Hey, H. Hoskins, J. Peirce, J. Phillips, and C. Tapscott, The Bouvet triple junction, *J. Geophys. Res., 81,* 1857-1869, 1976.

Searle, R. C., The active part of the Charlie-Gibbs fracture zone: A study using sonar and other geophysical techniques, *J. Geophys. Res., 86,* 243-262, 1981.

Shaw, P. R., and S. C. Cande, High-resolution inversion for South Atlantic plate kinematics using joint altimeter and magnetic anomaly data, *J. Geophys. Res., 95,* 2625-2644, 1990.

Smith, W. H. F., and D. T. Sandwell, Global sea floor topography from satellite altimetry and ship soundings, *Science, 277,* 1956-1962, 1997.

Solomon, S.C., P.Y. Huang, and L. Meinke, The seismic moment budget of slowly spreading ridges, *Nature, 334,* 58-60, 1988.

Taylor, B., K. Crook, and J. Sinton, Extensional transform zones and oblique spreading centers, *J. Geophys. Res., 99,* 19,707-19,718, 1994.

Tchalenko, J.S., Similarities between shear zones of different magnitudes, *Geol. Soc. Am. Bull., 81,* 1625-1640, 1970.

Tucholke, B. E., and H. Schouten, Kane Fracture Zone, *Mar. Geophys. Res., 10,* 1-39, 1989.

Tucholke, B. E., J. Lin, and M. C. Kleinrock, Megamullions and mullion structure defining oceanic metamorphic core complexes on the Mid-Atlantic Ridge, *J. Geophys. Res., 103,* 9857-9866, 1998.

Tuckwell, G. W., J. M. Bull, and D. J. Sanderson, Models of fracture orientation at oblique spreading centres, *J. Geol. Soc. London, 153,* 185-189, 1996.

Wessel, P., and W. H. F. Smith, Free software helps map and display data, *Eos Trans. AGU, 72,* 441, 1991.

Wetzel, L. R., D. A. Weins, and M. C. Kleinrock, Evidence from earthquakes for bookshelf faulting at large non-transform offsets, *Nature, 362,* 235-237, 1993.

White, R. S., R. S. Detrick, M. C. Sinha, and M. H. Cormier, Anomalous seismic crustal structure of oceanic fracture zones, *Geophys. J. R. Astron. Soc., 79,* 779-798, 1985.

Wilcox, R., T. Harding, and D.R. Sealy, Basic wrench tectonics, *Assoc. Pet. Geol. Bull., 57,* 74-96, 1973.

G. Carrara and P. Fabretti, Istituto di Geologia Marina, Consiglio Nazionale delle Ricerche, via Gobetti 101, 40129 Bologna, Italy.

R. A. Livermore, British Antarctic Survey, High Cross, Madingley Rise, Cambridge CB3 0ET, England. (ral@pcmail.nbs.ac.uk)

N. C. Mitchell, Department of Earth Sciences, Cardiff University, PO Box 914, Cardiff CF10 3YE, Wales. (neilm@carth.ox.ac.uk)

(Received January 21, 1999; revised September 27, 1999;
accepted November 5, 1999.)